Electronic Structure Tunability by Periodic *Meta*-Ligand Spacing in One-Dimensional Organic Semiconductors

Ignacio Piquero-Zulaica,[*,†] Aran Garcia-Lekue,[‡,¶] Luciano Colazzo,[‡] Claudio K. Krug,[§] Mohammed S. G. Mohammed,[‡,†] Zakaria M. Abd El-Fattah,[∥,⊥] J. Michael Gottfried,[§] Dimas G. de Oteyza,[†,‡,¶] J. Enrique Ortega,[†,‡,#] and Jorge Lobo-Checa[*,@,△]

†*Centro de Física de Materiales CSIC/UPV-EHU-Materials Physics Center, Paseo Manuel Lardizabal 5, E-20018 San Sebastián, Spain*

‡*Donostia International Physics Center (DIPC), Paseo Manuel Lardizabal 4, E-20018 Donostia-San Sebastián, Spain*

¶*Ikerbasque, Basque Foundation for Science, 48011 Bilbao, Spain*

§*Fachbereich Chemie, Philipps-Universität Marburg, Hans-Meerwein-Str. 4, 35032 Marburg, Germany*

∥*ICFO-Institut de Ciencies Fotoniques, The Barcelona Institute of Science and Technology, 08860 Castelldefels, Barcelona, Spain*

⊥*Physics Department, Faculty of Science, Al-Azhar University, Nasr City, E-11884 Cairo, Egypt*

#*Dpto. Física Aplicada I, Universidad del País Vasco, E-20018 San Sebastián, Spain*

@*Instituto de Ciencia de Materiales de Aragón (ICMA), CSIC-Universidad de Zaragoza, E-50009 Zaragoza, Spain*

△*Departamento de Física de la Materia Condensada, Universidad de Zaragoza, E-50009 Zaragoza, Spain*

E-mail: ipiquerozulaica@gmail.com; jorge.lobo@csic.es

Phone: +34 943 01 87 56 ; +34 876 55 33 53

Abstract

Designing molecular organic semiconductors with distinct frontier orbitals is key for the development of devices with desirable properties. Generating defined organic nanostructures with atomic precision can be accomplished by on-surface synthesis. We use this 'dry' chemistry to introduce topological variations in a conjugated poly-(*para*-phenylene) chain in the form of *meta*-junctions. As evidenced by STM and LEED, we produce a macroscopically ordered, monolayer thin zigzag chain film on a vicinal silver crystal. These cross-conjugated nanostructures are expected to display altered electronic properties, which are now unravelled by highly complementary experimental techniques (ARPES and STS) and theoretical calculations (DFT and EPWE). We find that *meta*-junctions dominate the weakly dispersive band structure, while the bandgap is tunable by altering the linear segment's length. These periodic topology effects induce significant loss of the electronic coupling between neighboring linear segments leading to partial electron confinement in the form of weakly coupled Quantum Dots. Such periodic quantum interference effects determine the overall semiconducting character and functionality of the chains.

Keywords

On-surface synthesis, cross-conjugated polymers, ultra-thin organic films, vicinal surfaces, electronic structure, electron confinement.

Conjugated polymers in the form of molecular chains are extensively used in industry as light emitting materials, photocatalysts, solar cells and biosensors due to their large and tunable bandgaps.[1–4] Control over their electronic properties is accomplished through topological functionalization of these π-conjugated oligophenylene chains, i.e. modification of their conductive pathways. In particular, changes of conjugation (from linear to cross-conjugation) by precise transitions from *para*- to *meta*-ligand substitutions[5,6] weaken the electronic communication between the repeating units of the polymer.[7] Such modifications

have also been described as quantum interference electron pathways,[8–10] and bear predicted effects such as scarcely dispersive bands,[5] wider bandgap ,[11] distinct optical properties,[4] electronic switching capabilites[12] and low conductance properties.[8–10,13,14] However, periodic *meta*-junction zigzag chains may also show enhanced charge mobility as compared to their poly-(*para*-phenylene) counterparts, reaching values comparable to those of amorphous silicon.[15]

Despite this wealth of industrially attractive properties of cross-conjugated polymers, key fundamental information, such as the predicted electronic structure awaits experimental validation. Such deficiency of fundamental knowledge limits the confidence in the existing predictions, according to which topology is expected to affect the electronic properties of the polymer. Several obstacles are responsible for the lack of the aforementioned experimental confirmation: i) the need of generating atomically identical chains exhibiting repeated *para*- to *meta*-ligand substituted units, ii) the synthesis of well-aligned chains, to be probed by non-local, averaging spectroscopies, iii) the minimization of lateral interactions, prone to affect their intrinsic band structure, and iv) the right choice of a support that sufficiently decouples the electronic signal from the investigated oligophenylene chains.

To overcome such obstacles, solutions can be found within the context of Surface Science. Particularly, the first prerequisite for obtaining perfectly reproducible cross-conjugated zigzag polymers can be accomplished by bottom-up on-surface synthesis. Surface-assisted C-C coupling processes have been recently applied to generate graphene nanoribbons (GNRs) with different edge terminations and widths,[16–21] and other types of oligophenylene chains.[22–25] Secondly, the chain alignment for non-local characterization can be achieved by the use of nanotemplated substrates, such as vicinal surfaces.[26–29] These special surfaces have been successfully used for the macroscopic alignment of carbon-based chains, a fundamental requirement for angle resolved photoemission (ARPES) experiments.[23,24,30,31] With respect to the minimization of lateral interchain coupling, this is an inherent feature of the Ullmann-type surface reactions[22] since the halogens are cleaved during the synthesis positioning them-

selves between neighboring chains.[23,24,32] These adatoms are reported to laterally decouple adjoining chains, without affecting the polymer's band structure, except for a minimal rigid energy shift similar to doping effects.[24,33] Finally, the substrate plays a fundamental role as a catalyst of the Ullmann reaction, making its choice crucial for a successful oligomer coupling. Good candidates that present excellent yields, control and reproducibility are the closed packed surfaces of coinage metals, which are extensively used for Ullmann-type surface reactions. Among these, silver stands out as a promising substrate, since it weakly interacts with the products while exhibiting large adsorbate diffusion rates.[34] Moreover, its *d*-bands are furthest from the Fermi level (below -3 eV), allowing a wide energy range for the study of the chain's band structure (see Figure S1 in S.I.).

In this work, we have overcome all the aforementioned obstacles and have generated an extended film of atomically precise zigzag chains on a vicinal Ag(111) surface, as evidenced by scanning tunneling microscopy (STM) and low energy electron diffraction (LEED). The electronic band structure of such films has been unravelled by means of ARPES and complemented by scanning tunneling spectroscopy (STS) measurements on Ag(111). In this way, we determine the experimental energy gap and visualize the spatial distribution of the frontier orbitals. Such wealth of experimental information has been clarified and expanded by a comprehensive set of density functional theory (DFT) calculations and electron plane wave expansion (EPWE) simulations.

Results and Discussion

We have produced a monolayer film of cross-conjugated zigzag chains from the surface polymerization of the 4,4"-dibromo-*meta* terphenyl (DMTP) molecular aromatic precursors *via* C-C coupling (see Figure 1a and Methods section). The template of choice is a vicinal Ag(111) crystal surface with linear, monoatomic steps running parallel to the [11-2] direc-

tion[29] that corresponds to the so-called fully-kinked (100% kinked) configuration of the step-edge. We used this particular substrate since it provides a higher flexibility to reconstruct and therefore accommodate the produced zigzag structures more efficiently (cf. Methods section and Figure S1 in S.I.). Indeed, we can already disclose that we achieved an excellent film featuring a high yield of well-ordered and aligned zigzag chains.

The formed zigzag chains appear practically planar on the surface (Figure 1b) and are covalently bonded displaying the characteristic phenyl-phenyl distance of $a \sim 4.3$ Å along the straight segments and a superperiodicity of $L \sim 2.24$ nm between equivalent elbows.[22,35] The unit cell of the chain features two straight subunits made up of two phenyl rings (in *para*-positions) linked to two edge rings acting as *meta*-junctions (Figure 1a). Note that in the STM image these chains are separated by spherical features attributed to Br atoms split off from the precursor molecules at the initial step of the on-surface reaction.[36–43] The LEED pattern reveals that the organic chains are aligned parallel to the steps and show long-range order as they are commensurate with the underlying substrate (Figure 1b and Figure S2 in S.I.). Particularly, the main silver diffraction spots (red and green circles) are surrounded by a set of spots aligned along the average step direction yielding a (9, 5; 0, 4) superstructure.

Our STM and LEED structural results contain the required ingredients (atomic precision of the structure, defined alignment, long-range order and minimization of lateral interactions by Br adatom presence) to expect the existence of a defined and coherent electronic band structure from these chains. Figures 1c-e show the second derivative (to enhance the details) of the ARPES spectral weight obtained from such a film saturating the surface (raw data is shown in Figure S3 of the S. I.). The resulting electronic structure in the direction parallel to the average step direction and the main axis of the zigzag chains (E vs k_y with $k_x = 0.1$ Å^{-1}), exhibits weakly dispersive bands between -1.8 eV and -3.5 eV, separated by a ~ 0.6 eV gap (cf. Figure 1c). None of these ARPES features are observable on the pristine substrate (cf. Figure S1 in S.I.). A closer inspection reveals that each one of them consists

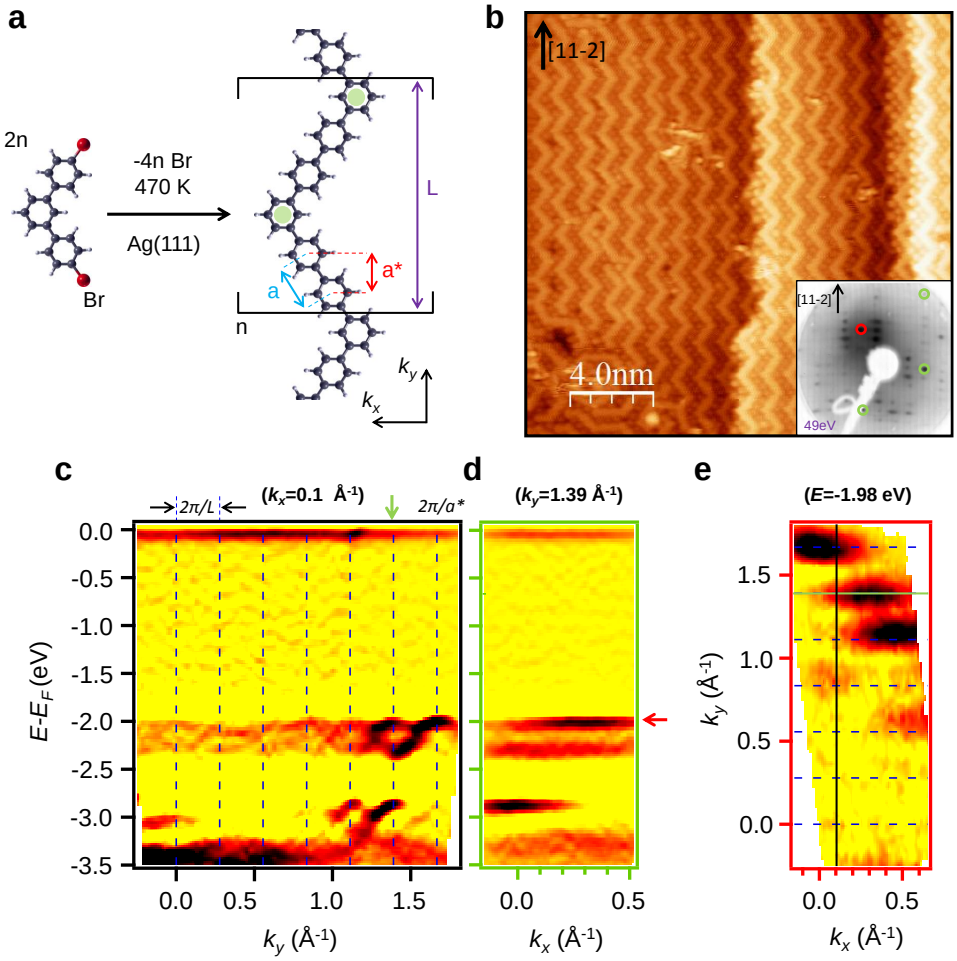

Figure 1: Structural arrangement and ARPES electronic band structure of the zigzag chain film grown on a vicinal Ag(111) surface. (a) Schematic representation of the DMTP precursor and the resulting zigzag covalent chain, showing its characteristic lenghts: phenyl-phenyl distance (a) and its projection along the chain's average direction (a^*), and polymer superperiodicity (L). (b) High resolution STM image after chain synthesis on a vicinal plane $\sim 3.6°$ off from the (111) crystal position. The zigzag chains are separated by Br atoms and preferentially follow the step parallel direction ([11-2]). (STM parameters: $V = -394$ mV, $I = 234$ pA, $T_{sample} = 100$ K). Inset shows the LEED pattern after chain formation that exhibits single-domain, well-aligned arrangement. The superstructure spots are in registry with the circled main spots (in red the (0,0) and in green the substrate's first order diffractions), implying commensurability with the terrace atoms (LEED parameters: $E_{kin} = 49$ eV, $T_{sample} = 300$ K). (c) ARPES experimental band structure of *meta*-junctioned cross-conjugated zigzag chains parallel to the average direction of chains and steps (E vs k_y with $k_x = 0.1$ Å^{-1}). (d) Experimental band structure perpendicular to the chain average axis (E vs k_x, with $k_y = 1.39$ Å^{-1} indicated by green arrow in (c)). (e) Isoenergetic cut (k_x vs k_y) at the top of the valence molecular band ($E = -1.98$ eV, marked by red arrow in (d)). The second derivative of the intensity is shown in a linear color scale (highest being black). (ARPES parameters: $h\nu = 21.2$ eV, $T_{sample} = 150$ K).

of a pair of anti-phase oscillatory bands (Figs. S3 and S4 in S.I.). The spectral intensity peaks around $2\pi/a^*$, where a^* represents the projected phenyl-phenyl distance along the average chain direction (Figure 1a), assuring its molecular origin.[44] The faint replicas with $2\pi/L$ periodicity (vertical dashed blue lines), stem from the zigzag chain superperiodicity L (Figure 1a), in agreement with the STM dataset.

The 1D nature of these zigzag chains is demonstrated by the lack of dispersion perpendicular to the average chain axis. Figure 1d shows a representative cut (E vs k_x) across the center of the 6$^{\text{th}}$ Brillouin zone (green arrow at k_y=1.39 Å^{-1} in Figure 1c), where discrete flat bands can be observed. This confirms that they stem from different molecular orbitals of the zigzag polymer.[45] The non-dispersive character at the top of the valence band (red arrow at -1.98 eV) can also be traced from the isoenergetic cut (k_x vs k_y) shown in Figure 1e, where 1D polymer bands replicate at each Brillouin zone center, gaining intensity for the larger k_y values. These photoemission intensity modulations have been simulated with the EPWE method,[46,47] which confirms that these features are neither affected by the templating Ag surface nor by the presence of Br atoms intercalated between the chains (see Methods section and Figure S4 in S.I.). Indeed, we experimentally find that the presence of Br embedded in between the zigzag chains only causes a rigid shift of the molecular band structure by 200$\pm$50 meV to higher energy, according to Figure S5 of the S.I. and in agreement with previous work .[24,33]

Our ARPES results suggest that the zigzag chains are largely decoupled from the metallic substrate since the observed molecular bands do not show signs of hybridization with the substrate in that energy window. Besides, the chains are semiconducting in nature with a bandgap certainly larger than 2 eV, since no other bands closer to the Fermi energy are observed in the occupied region. The band structure strongly contrasts with that of the poly-(*para*-phenylene) (called PPP hereafter) chains, which exhibits a single, highly dispersive molecular band across the entire Brillouin zone[23–25] (Figure S6 in S.I.). Instead, it closely resembles the one predicted for poly-(*meta*-phenylene) (called PMP hereafter) chains,[5] im-

plying that the presence of *meta*-junctions strongly modifies the electronic structure of a polymeric chain[13] (cf. Fig S7 of S.I.).

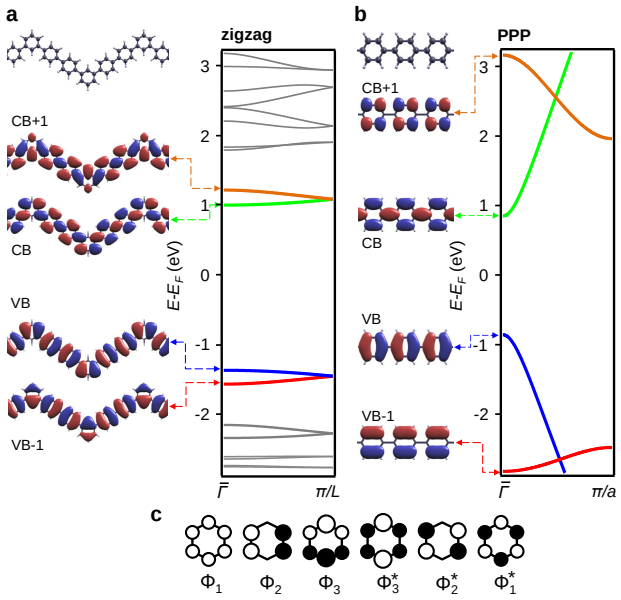

Figure 2: Comparison of molecular orbital shape and band structure between zigzag chains and straight PPP chains, as obtained from DFT calculations. The right plots in (a) and (b) show the calculated electronic band structure, where (a) corresponds to the zigzag polymer and (b) to PPP. The highly dispersive character of the PPP bands contrasts with the practically flat bands of the zigzag chains, accompanied by a notable difference in the frontier orbital bandgap. Left panels in (a) and (b) show the spatially resolved molecular orbitals at $\bar{\Gamma}$ for each band. In a simplistic view, they are constructed by overlapping different benzene molecular orbitals, which are schematically shown in (c).

The weak interaction observed between the zigzag chain film and the substrate is a favorable playground for a systematic theoretical analysis. As a first approximation, we consider the polymers as free-standing and planar. On this basis, we use DFT calculations to corroborate the weakly dispersive band structure observed experimentally. The calculated electronic structure shown in Figure 2a exhibits convincing qualitative agreement with the experimental data. In particular, the dispersive character of the first four valence bands (VBs) of the zigzag chain (between -1 eV and -2.5 eV) is consistent with that in Figure 1c. The energy mismatch can be attributed to the absence of a substrate in the calculations, as well as to the well-known limitation of DFT to accurately predict HOMO-LUMO gaps. Note that the

calculated bands span from the $\bar{\Gamma}$ point to the Brillouin zone boundary (π/L), which in the experiment appears 12 times replicated until $2\pi/a^*$. For comparison, the calculations are extended to straight PPP chains (Figure 2b) which strongly differ in the electronic structure by exhibiting a highly dispersive single VB in the same energy window. Moreover, the zigzag chain exhibits a greater bandgap than its straight counterpart, confirming the enhanced semiconductive character of the former (see figure S7 in S.I.).

The experimental value of the frontier orbital bandgap of the zigzag chains can be obtained by low-temperature (4 K) STS. For such measurements we deposit a submonolayer coverage of DMTP molecules on Ag(111) so that small zigzag island patches are formed on the surface while still allowing access to the bare substrate for tip calibration and treatment (Figure 3 and Fig. S5 in S.I.). Figure 3a shows the dI/dV spectra at the center (red) of a straight arm of a zigzag chain (see figure inset) and the Ag substrate (grey). The VB onset is detected close to -2.1 V (coinciding with the ARPES value in Figure 1d) while the conduction band (CB) edge is around 1.6 V resulting in an overall bandgap of $\sim$ 3.7 V. Therefore this value is larger than the 3.2 V reported for PPP chains grown on Au(111)[42] and confirms the enhanced semiconducting character of the zigzag chains.

DFT calculations can also shed light onto the effect that the periodically spaced *meta*-junctions have on the overall electronic structure by comparing the spatially resolved molecular orbitals at the $\bar{\Gamma}$ point with the π molecular orbitals of benzene (Figure 2c). In the PPP case (Figure 2b), VB and CB are constructed by the overlap of Φ_3 and Φ_3^* benzene molecular orbitals, respectively. These orbitals present a large electronic weight on the carbon atoms linking the phenyl rings (*para*-positions), giving rise to highly dispersive valence and conduction bands. Likewise, the less dispersive character of the VB-1 and CB+1 bands can be attributed to the orbital set that exhibits a nodal plane through the *para* carbon atoms (Φ_2 and Φ_2^* orbitals). Contrarily, for the zigzag chains (Figure 2a) the VB and CB are a combination of two degenerate orbitals.[7] In particular, the VB is made up of Φ_3 (straight

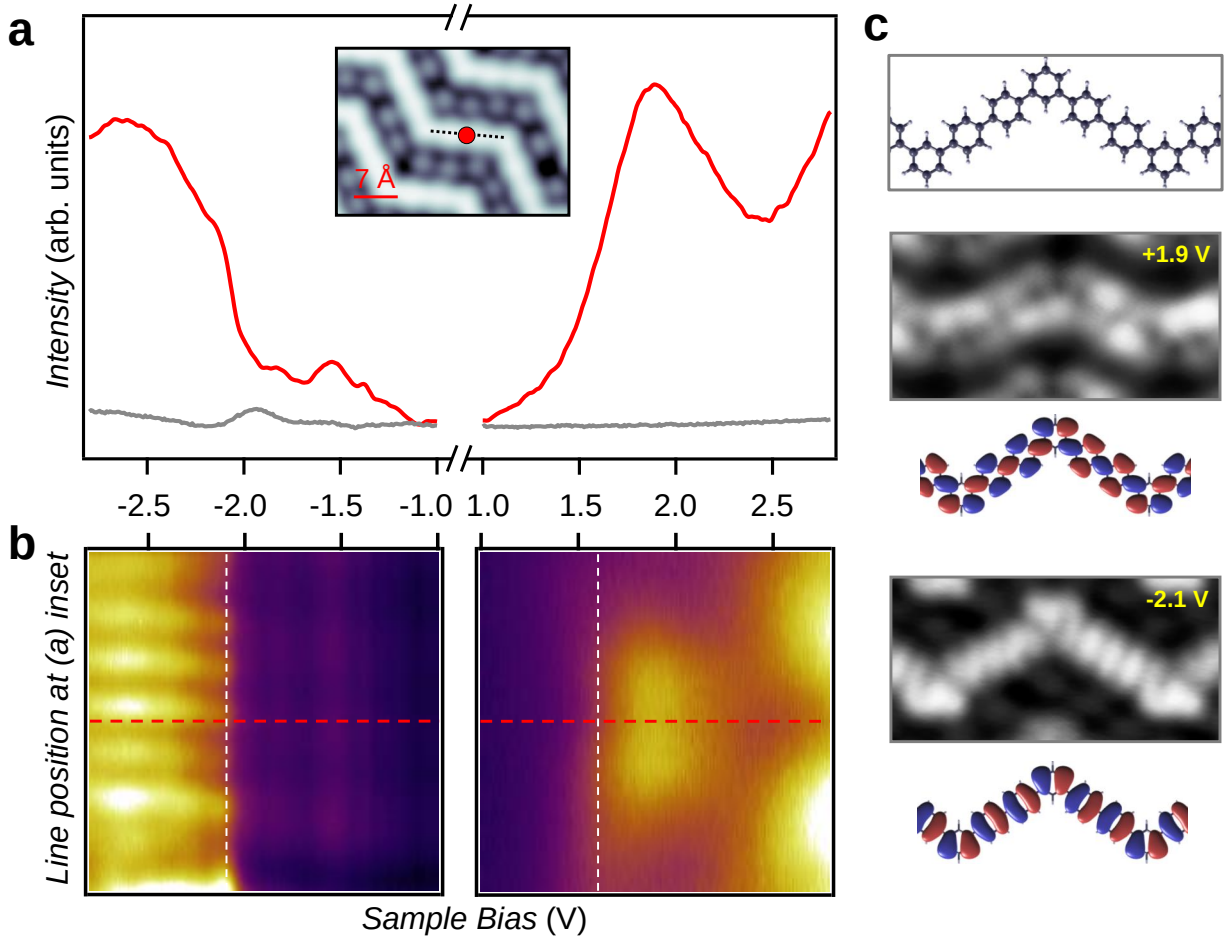

Figure 3: STS experimental determination of the zigzag chain's frontier orbitals on Ag(111). (a) Constant-height dI/dV spectra acquired at the center of a zigzag straight arm (red point in STM image inset) and substrate (grey) (STM imaging parameters: 50 mV, 100 pA; frame: 3.6 × 2.5 nm^2). (b) Constant-height dI/dV linescan spectra along the zigzag arm (indicated by a dotted line in the STM topography inset) for the same bias range of panel (a). The onsets of the VB and CB are clearly defined (vertical dashed white lines), yielding a bandgap of $\sim$ 3.7 eV (STS bias voltage modulation for (a) and (b): 10 mV_{rms} at 341 Hz. Close-feedback parameters: -350 mV, 150 pA and 1200 mV, 100 pA for the negative and positive resonances regions, respectively). (c) From top to bottom: ball and stick model of the zigzag chain. High-resolution dI/dV maps acquired at constant-height with a CO functionalized STM tip at 1.9 V and -2.1 V, i.e. close to the CB and VB onsets (frames: 3.0 × 1.5 nm^2; bias voltage modulation 10 mV_{rms} at 341 Hz). Underneath each map the corresponding DFT gas phase molecular frontier orbitals are shown for comparison.

sections) and Φ_2 (elbows) orbitals, which is mirrored in the CB by Φ_3^* (straight sections) and Φ_2^* (elbows). This orbital mixing, along with the reduced orbital amplitude at the *meta*-positions and expected phase shifts induced by momentum steering at the elbows, results in a diminished orbital interaction (overlap) that leads to a severe weakening of the electron coupling between adjacent straight segments. Indeed, the flat band character is also exhibited by the VB-1 and CB+1, even though they mostly arise from a single type of benzene molecular orbital coupling (Φ_3 and Φ_3^*, respectively). This strong electronic effect governed by the *meta*-junction is generally referred to as cross-conjugation[5,6] or destructive quantum interference.[8–10,14]

The reduced electronic coupling between neighboring linear segments causes electron localization, an effect that can be adequately addressed with STS. Figure 3b presents a color plot representing stacked dI/dV point spectra measured along a single straight segment (black dashed line in the inset of Fig. 3a). Aside from clearly visualizing an overall bandgap of 3.7 eV, we observe confinement in the CB within such segments where the spatial modulations in the local density of states (LDOS) are consistent with the first two stationary states of a particle in a box. In particular, their amplitudes die away at the edges of the linear segments (elbow positions of the zigzag chains) but the lower state at 1.9 V features an antinode at the segment's center (the peak in the red spectrum of Fig. 3a), whereas the second state at 2.5 V oppositely exhibits a node at that position. Such electron confinement effects have also been observed in related structures, as in the case of finite size PPP chains featuring a single elbow (in *meta*-junction)[13] or in closed-cycle geometries of honeycombenes.[48] In essence, we can conclude that *meta*-junctions act as scattering barriers for the polymer electrons regardless of the overall geometry, i.e. as closed structures[48] or as edged (non-linear) chains.[13]

Once we have verified that each straight segment of our zigzag chains acts as a confining unit, reminiscent of a 1D array of weakly interacting Quantum Dots (QDs),[49] it should be possible to tune their electronic properties by modulating the straight segment's

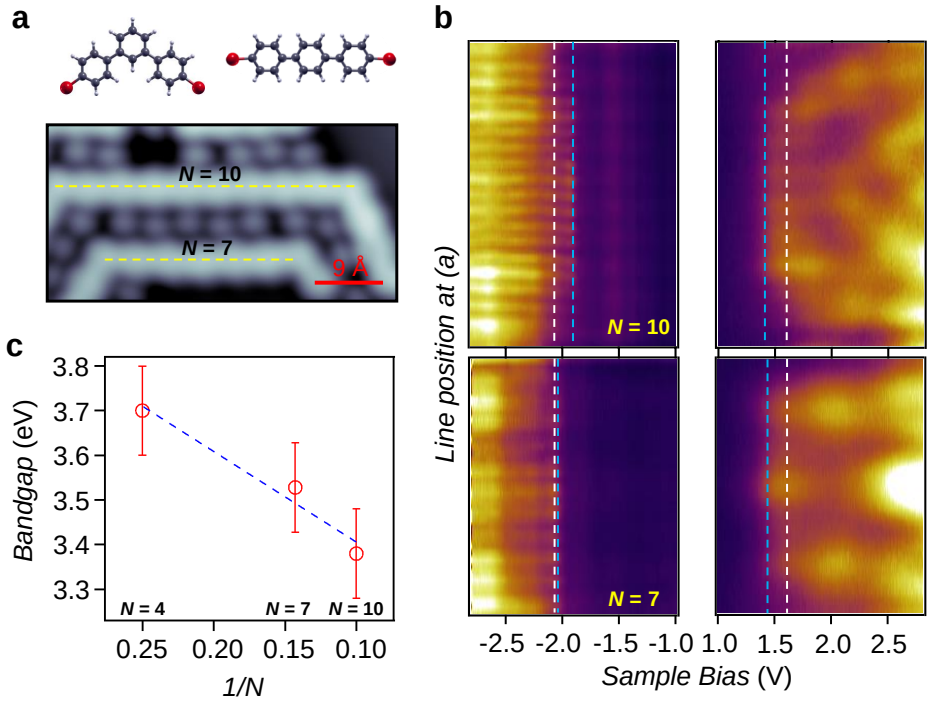

Figure 4: Tuning the electronic confined states through the linear segment's length (QD size). (a) Schematic representation of the co-evaporated molecular precursors (DMTP and DBTP) that generate longer straight segments between the *meta*-coordinating phenyls. The STM image shows two longer linear segments of 7 and 10 phenyl rings between elbows (Imaging parameters: 50 mV, 100 pA; frame: 4.5 × 2.3 nm^2). (b) Constant-height dI/dV line profiles close to the VB and CB onsets along the two segments following the dashed lines in (a). The intensity modulation of the CB confirms the confinement nature of the *meta*-junction termination. Furthermore, the frontier orbital bandgap (vertical dashed blue lines) is reduced compared to the N=4 case, which is indicated by the two vertical dashed white lines. (STS parameters: bias voltage modulation of 10 mV$_{rms}$ at 341 Hz; close-feedback at -350 mV, 150 pA and 1200 mV, 120 pA for the negative and positive resonances regions, respectively). (c) Experimental bandgap extracted from the STS line profiles revealing a $1/N$ behavior (compare to Figure S8 in S.I.).

length. Varying the 1D QD length should affect the energy levels as well as the corresponding frontier orbital bandgap. To do so, we co-evaporated on Ag(111) linear precursors (DBTP molecules[24]) together with the previously used ones to generate the zigzag chains, as shown in Figure 4a. The Ullmann coupling reaction is likewise activated by post-annealing to 470 K, resulting in linear segments of phenyl length configurations of $N = 4+3n$ (N being the total phenyl number and n the amount of DBTP precursors embedded in the straight segment). Figure 4b shows color plots of the dI/dV linescan for $N = 7$ (bottom) and $N = 10$ (top) QDs, which evidence the expected squared wavefunction intensity variations in the CBs for the same energy range as Figure 3b. Most importantly, by comparison to the dashed white lines corresponding to the $N = 4$ segment, we observe that the bandgap shrinks as the size of the segment increases (dashed blue lines). A quantitative analysis of the experimentally determined bandgap is shown in Figure 4c, revealing a $1/N$ behavior in agreement with previous work for similar chains.[13] Such behavior matches our DFT calculations for planar, free-standing, periodic zigzag chains of different straight segment length, which confirm not only that the bandgap of the cross-conjugated zigzag chains is larger than the one of its linear PPP counterpart, but it is also tunable as $1/N$ (cf. Figures S7 and S8 in S.I.).

Finally, we should discuss an additional property of this system that may affect the frontier orbital bandgap: the relative twisting of the phenyl rings (non-planar chain morphology). Figure 3c shows high-resolution constant height dI/dV maps close to the valence and conduction band onsets, namely at -2.1 eV and 1.9 eV, respectively. Both maps replicate well the molecular orbital simulations of Figure 2a, which are calculated for planar structures and are depicted below for direct comparison. While the slight discrepancies in nodal positions are attributed to the CO probe functionalization,[50] the intensity variations are in turn ascribed to the twisting of the phenyl rings.[42] The phenyl twisting is confirmed from constant height bond resolution imaging with a CO functionalized tip,[51] on which we find subtle intensity modulations on the external parts of the phenyl rings (see Fig. S9 of S.I.) indicative of such

phenyl twisting. This is in agreement with previous work that found $\sim 20°$ phenyl twisting on PPP chains with respect to the surface plane.[24] To determine the effect of the twisting on the frontier orbital bandgap, we have performed DFT calculations for free-standing zigzag chains and obtained an energy minimum close to 30° phenyl twisting of the zigzag chain. However, the calculations show that the electronic bandgap is scarcely increased compared to the planar configuration. Given that the underlying substrate is known to decrease the phenyl twisting by flattening the chains, we expect this effect to be smaller than ~ 200 meV (cf. Figure S10 in the S.I.), validating the use of free-standing, planar configuration geometries in the DFT calculations that support our findings.

Conclusions

We have been able to synthesize and macroscopically align a saturated film of cross-conjugated oligophenylene zigzag chains on a vicinal Ag(111) surface. We find that these atomically precise chains remain sufficiently decoupled from each other and from the substrate to probe their elusive band structure with ARPES, revealing weakly dispersing one-dimensional electronic bands along the chain direction. DFT band structure calculations and EPWE photoemission intensity simulations satisfactorily reproduce our experimental findings. By means of STS, we find that the zigzag chain has a larger frontier orbital bandgap than its straight counterpart (PPP) and observe electronic confinement in each straight segment of the zigzag chains, reminiscent of 1D arrays of weakly interacting QDs. Such states can be tuned by changing the length of the straight segments, affecting the frontier orbital bandgap, which follows a $1/N$ dependency. Indeed, our molecular orbital simulations confirm that the periodically spaced *meta*-junctions at the elbows of the zigzag chain are the main structural feature responsible for the reduction of electronic coupling between adjacent linear segments. These findings corroborate the important effects that the conductive path topology of a molecular

wire has on its frontier orbitals, which are responsible for defining its chemical, optical and electronic properties. Recent advances in transfer techniques ensure that on-surface synthesized and well-aligned organic nanostructures can be collectively transferred onto insulating substrates maintaining their relative arrangement,[52–54] which opens the path to further study the transport and optical properties of these cross-conjugated oligophenylene zigzag chains.

Methods

A silver crystal surface curved around the (645) direction was used as tunable vicinal substrate for chain formation and alignment.[29] This curved sample exhibits (111) terraces of variable size (position dependent on its curvature) separated by monoatomic steps oriented along the [11-2] direction. The steps are of fully-kinked type, in which out-protruding atoms have no side neighbors (Figure S1 in S.I). Notably, periodic roughening of such step-edges bears negligible energy cost, and hence can readily accommodate to the zigzag structure of the chains.[29] The saturated zigzag film that presents best order was observed at the vicinal plane $\sim 3.6^{\circ}$ from the (111) region, corresponding to an average terrace size of 3.8 nm. The ARPES data shown in Figure 1 and Figures S1, S3, S4 and S6 in S.I. corresponds to this position of the substrate. The sample was cleaned by repeated cycles of Ar^{+} sputtering at energies of 1.0 keV, followed by annealing at 700 K. This produced clean and well-ordered surface step arrays as verified by the splitting of the LEED spots along the surface curvature.

The *meta*-junctioned haloaromatic compound, DMTP, was sublimated from a Knudsen cell at 360 K at a low flux (1 ML/hour) while the sample was held at 470 K.[22,48,55] Covalently bonded zigzag chains appeared separated by Br adatoms, suggesting some influence from the latter in steering chain growth and alignment. The step flexibility promoted the chain formation while keeping other irregular structures or hyperbenzene macrocycles to a

minimum.[41] The structures remained densely packed up to high temperatures ($\sim$ 600 K), beyond which halogen desorption starts, accompanied by chain misalignment.[18,56]

ARPES measurements were performed with a lab-based experimental setup using a display-type hemispherical electron analyzer (SPECS Phoibos 150, energy/angle resolution of 40 meV/0.1°) combined with a monochromatized Helium I ($h\nu$=21.2 eV) source. Measurements were acquired with the sample at 150 K by moving the polar angle, which is set to be parallel to the average step direction.

The STM measurements on the curved Ag(111) crystal were carried out at 100 K using a variable temperature Omicron STM with a Nanonis SPM control system. The bias voltages given in the manuscript refer to a grounded tip. STM data were acquired in constant current mode and were processed with the WSxM software.[57]

LT-STM/STS measurements were performed with a commercial Scienta-Omicron low temperature system, operating in ultrahigh vacuum (UHV) at 4.3 K. For the measurement, the bias voltage was applied to the tip while the sample was electronically grounded. The STM tip was prepared *ex-situ* by clipping a Pt/Ir wire (0.25 mm) and sharpened *in-situ* by repeatedly indenting the tip a few nanometers (1 to 4 nm) into the Ag surface while applying bias voltages from 2 V to 4 V between tip and sample. In order to perform bond-resolved STM imaging, the tip apex was terminated with a CO molecule, directly picked up from the surface, by positioning the sharp metal tip on top of it and applying a 500 ms bias pulse at -2 V. The imaging was performed by measuring at constant height while applying a bias voltage to the tip within the range of 2.0 mV and 3.5 mV. For spectroscopic point spectra and conductance maps, the dI/dV signals were measured by a digital lock-in amplifier (Nanonis). STM images were analyzed by using the WSxM software.[57]

Ab-initio calculations were carried out using density functional theory (DFT), as imple-

mented in the SIESTA code.[58] The optB88-vdW functional,[59] which accounts for non-local corrections, was adopted for the exchange and correlation potential. For each organic nanostructure, we considered a supercell consisting of a chain infinite along the x axis, with vacuum gaps of 15 Å in y and z directions in order to avoid interactions between chains in adjacent cells. A Monkhorst-Pack k-point grid with 20x1x1 k-points was used for the Brillouin zone sampling and the mesh cut-off for real space integrations was set to 300 Ry. We employed a double-ξ plus polarization (DZP) basis set, and a mesh-cutoff of 300 Ry for the real-space integrations. All structures were fully relaxed until residual forces were less than 0.01 eV/ Å.

The Electron-Plane-Wave-Expansion (EPWE) method, which was recently used to describe the electronic properties of graphene nanostructures,[47] is employed to simulate ARPES data. Within the EPWE approach, the photoemission intensity for a given binding energy and photoelectron wave vector is obtained from Fermi's golden rule applied to the in-plane wave function (an initial state) and a normalized plane wave (a final state) for the parallel component of the photoelectron wave function, as detailed in Ref. [47]. In this semiempirical method, zigzag chains are considered free-standing and planar, which implies that the simulated bands are substrate independent and free of Br interactions.

Acknowledgement

I.P-Z thanks Dr. Jens Brede for fruitful discussion. Z.M.A. thanks Prof. F. J. García de Abajo for providing the EPWE code. We acknowledge the financial support from the Spanish Ministry of Economy, Industry and Competitiveness (MINECO, Grant No. MAT2016-78293-C6), from the Basque Government (Grant No. IT-621-13), from the regional Government of Aragon (RASMIA project), from the European Regional Development Fund (ERDF) under the program Interreg V-A España-Francia-Andorra (Contract No. EFA 194/16 TNSI),

from the German Science Foundation (DFG) through the CRC 1083 and Grant No. GO 1812/2 and funding from the European Research Council (ERC) under the European Union's Horizon 2020 research and innovation programme (grant agreement no. 635919).

Supporting Information Available

Additional information and 10 figures can be found in the S.I. This material is available free of charge *via* the Internet at XXXXXX

Author Information

Corresponding Author

*E-mail: (I.P-Z) ipiquerozulaica@gmail.com and (J.L-C) jorge.lobo@csic.es

Author Contributions

I.P-Z., J.L-C. and C.K.K. conducted the experimental measurements of the saturated film (ARPES, STM and LEED) and corresponding data analysis; L.C., I.P-Z., M.S. and D.G.O. performed LT-STM/STS measurements of the partially covered surface; A.G-L. performed the DFT calculations and Z.M.A. performed EPWE simulations; I.P-Z. and J.L-C. wrote the manuscript. All authors contributed to the revision and final discussion of the manuscript; I.P-Z., J.L-C., J.E.O. and J.M.G. conceived this project.

Notes

The authors declare that they have no competing financial interests.

References

(1) Günes, S.; Neugebauer, H.; Sariciftci, N. S. Conjugated Polymer-Based Organic Solar Cells. *Chem. Rev.* **2007**, *107*, 1324–1338.

(2) Li, G.; Chang, W.-H.; Yang, Y. Low-Bandgap Conjugated Polymers Enabling Solution-Processable Tandem Solar Cells. *Nat. Rev. Mater.* **2017**, *2*, 17043.

(3) Masai, H.; Terao, J. Stimuli-Responsive Functionalized Insulated Conjugated Polymers. *Polym. J.* **2017**, *49*, 805–814.

(4) Guiglion, P.; Zwijnenburg, M. A. Contrasting the Optical Properties of the Different Isomers of Oligophenylene. *Phys. Chem. Chem. Phys.* **2015**, *17*, 17854–17863.

(5) Hong, S. Y.; Kim, D. Y.; Kim, C. Y.; Hoffmann, R. Origin of the Broken Conjugation in m-Phenylene Linked Conjugated Polymers. *Macromolecules* **2001**, *34*, 6474–6481.

(6) van der Veen, M.; Rispens, M.; Jonkman, H.; Hummelen, J. Molecules with Linear π-Conjugated Pathways between All Substituents: Omniconjugation. *Adv. Funct. Mater.* **2004**, *14*, 215–223.

(7) Kocherzhenko, A. A.; Grozema, F. C.; Siebbeles, L. D. A. Single Molecule Charge Transport: From a Quantum Mechanical to a Classical Description. *Phys. Chem. Chem. Phys.* **2011**, *13*, 2096–2110.

(8) Manrique, D. Z.; Huang, C.; Baghernejad, M.; Zhao, X.; Al-Owaedi, O. A.; Sadeghi, H.; Kaliginedi, V.; Hong, W.; Gulcur, M.; Wandlowski, T.; Bryce, M. R.; Lambert, C. J. A Quantum Circuit Rule for Interference Effects in Single-Molecule Electrical Junctions. *Nat. Commun.* **2015**, *6*, 6389.

(9) Guédon, C. M.; Valkenier, H.; Markussen, T.; Thygesen, K. S.; Hummelen, J. C.; van der Molen, S. J. Observation of Quantum Interference in Molecular Charge Transport. *Nat. Nanotechnol.* **2012**, *7*, 305–309.

(10) Markussen, T.; Stadler, R.; Thygesen, K. S. The Relation between Structure and Quantum Interference in Single Molecule Junctions. *Nano Lett.* **2010**, *10*, 4260–4265.

(11) Limacher, P. A.; Lüthi, H. P. Cross-Conjugation. *Wiley Interdiscip. Rev. Comput. Mol. Sci.* **2011**, *1*, 477–486.

(12) Thompson, A. L.; Ahn, T.-S.; Thomas, K. R. J.; Thayumanavan, S.; Martínez, T. J.; Bardeen, C. J. Using Meta Conjugation To Enhance Charge Separation versus Charge Recombination in Phenylacetylene Donor-Bridge-Acceptor Complexes. *J. Am. Chem. Soc.* **2005**, *127*, 16348–16349.

(13) Wang, S.; Wang, W.; Lin, N. Resolving Band-Structure Evolution and Defect-Induced States of Single Conjugated Oligomers by Scanning Tunneling Microscopy and Tight-Binding Calculations. *Phys. Rev. Lett.* **2011**, *106*, 206803.

(14) Tada, T.; Yoshizawa, K. Molecular Design of Electron Transport with Orbital Rule: Toward Conductance-Decay Free Molecular Junctions. *Phys. Chem. Chem. Phys.* **2015**, *17*, 32099–32110.

(15) Terao, J.; Wadahama, A.; Matono, A.; Tada, T.; Watanabe, S.; Seki, S.; Fujihara, T.; Tsuji, Y. Design Principle for Increasing Charge Mobility of π-Conjugated Polymers Using Regularly Localized Molecular Orbitals. *Nat. Commun.* **2013**, *4*, 1691.

(16) Cai, J.; Ruffieux, P.; Jaafar, R.; Bieri, M.; Braun, T.; Blankenburg, S.; Muoth, M.; Seitsonen, A. P.; Saleh, M.; Feng, X.; Müllen, K.; Fasel, R. Atomically Precise Bottom-Up Fabrication of Graphene Nanoribbons. *Nature* **2010**, *466*, 470–473.

(17) Talirz, L.; Ruffieux, P.; Fasel, R. On-Surface Synthesis of Atomically Precise Graphene Nanoribbons. *Adv. Mater.* **2016**, *28*, 6222–6231.

(18) de Oteyza, D. G.; Garcia-Lekue, A.; Vilas-Varela, M.; Merino-Díez, N.; Carbonell-Sanromà, E.; Corso, M.; Vasseur, G.; Rogero, C.; Guitián, E.; Pascual, J. I.; Ortega, J. E.; Wakayama, Y.; Peña, D. Substrate-Independent Growth of Atomically Precise Chiral Graphene Nanoribbons. *ACS Nano* **2016**, *10*, 9000–9008.

(19) Corso, M.; Carbonell-Sanromà, E.; de Oteyza, D. G. In *On-Surface Synthesis II*; de Oteyza, D. G., Rogero, C., Eds.; Springer International Publishing: Cham, 2018; pp 113–152.

(20) Gröning, O.; Wang, S.; Yao, X.; Pignedoli, C. A.; Borin Barin, G.; Daniels, C.; Cupo, A.; Meunier, V.; Feng, X.; Narita, A.; Müllen, K.; Ruffieux, P.; Fasel, R. Engineering of Robust Topological Quantum Phases in Graphene Nanoribbons. *Nature* **2018**, *560*, 209–213.

(21) Rizzo, D. J.; Veber, G.; Cao, T.; Bronner, C.; Chen, T.; Zhao, F.; Rodriguez, H.; Louie, S. G.; Crommie, M. F.; Fischer, F. R. Topological Band Engineering of Graphene Nanoribbons. *Nature* **2018**, *560*, 204–208.

(22) Fan, Q.; Wang, C.; Han, Y.; Zhu, J.; Hieringer, W.; Kuttner, J.; Hilt, G.; Gottfried, J. M. Surface-Assisted Organic Synthesis of Hyperbenzene Nanotroughs. *Angew. Chem. Int. Ed.* **2013**, *52*, 4668–4672.

(23) Vasseur, G. et al. Quasi One-Dimensional Band Dispersion and Surface Metallization in Long-Range Ordered Polymeric Wires. *Nat. Commun.* **2016**, *7*, 10235.

(24) Basagni, A.; Vasseur, G.; Pignedoli, C. A.; Vilas-Varela, M.; Peña, D.; Nicolas, L.; Vitali, L.; Lobo-Checa, J.; de Oteyza, D. G.; Sedona, F.; Casarin, M.; Ortega, J. E.; Sambi, M. Tunable Band Alignment with Unperturbed Carrier Mobility of On-Surface Synthesized Organic Semiconducting Wires. *ACS Nano* **2016**, *10*, 2644–2651.

(25) Abadía, M.; Ilyn, M.; Piquero-Zulaica, I.; Gargiani, P.; Rogero, C.; Ortega, J. E.; Brede, J. Polymerization of Well-Aligned Organic Nanowires on a Ferromagnetic Rare-Earth Surface Alloy. *ACS Nano* **2017**, *11*, 12392–12401.

(26) Ortega, J. E.; Mugarza, A.; Repain, V.; Rousset, S.; Pérez-Dieste, V.; Mascaraque, A. One-Dimensional versus Two-Dimensional Surface States on Stepped Au(111). *Phys. Rev. B* **2002**, *65*, 165413.

(27) Mugarza, A.; Schiller, F.; Kuntze, J.; Cordón, J.; Ruiz-Osés, M.; Ortega, J. E. Modelling Nanostructures with Vicinal Surfaces. *J. Phys.: Condens. Matter* **2006**, *18*, S27.

(28) Corso, M.; Schiller, F.; Fernández, L.; Cordón, J.; Ortega, J. E. Electronic States in Faceted Au(111) Studied with Curved Crystal Surfaces. *J. Phys.: Condens. Matter* **2009**, *21*, 353001.

(29) Ortega, J. E.; Vasseur, G.; Piquero-Zulaica, I.; Matencio, S.; Valbuena, M. A.; Rault, J. E.; Schiller, F.; Corso, M.; Mugarza, A.; Lobo-Checa, J. Structure and Electronic States of Vicinal Ag(111) Surfaces with Densely Kinked Steps. *New J. Phys.* **2018**, *20*, 073010.

(30) Ruffieux, P.; Cai, J.; Plumb, N. C.; Patthey, L.; Prezzi, D.; Ferretti, A.; Molinari, E.; Feng, X.; Müllen, K.; Pignedoli, C. A.; Fasel, R. Electronic Structure of Atomically Precise Graphene Nanoribbons. *ACS Nano* **2012**, *6*, 6930–6935.

(31) Senkovskiy, B. V.; Usachov, D. Y.; Fedorov, A. V.; Haberer, D.; Ehlen, N.; Fischer, F. R.; Grüneis, A. Finding the Hidden Valence Band of N = 7 Armchair Graphene Nanoribbons with Angle-Resolved Photoemission Spectroscopy. *2D Mater.* **2018**, *5*, 035007.

(32) Cai, L. et al. Direct Formation of C–C Double-Bonded Structural Motifs by On-Surface Dehalogenative Homocoupling of *gem* -Dibromomethyl Molecules. *ACS Nano* **2018**, *12*, 7959–7966.

(33) Merino-Díez, N.; Lobo-Checa, J.; Nita, P.; Garcia-Lekue, A.; Basagni, A.; Vasseur, G.; Tiso, F.; Sedona, F.; Das, P. K.; Fujii, J.; Vobornik, I.; Sambi, M.; Pascual, J. I.; Ortega, J. E.; de Oteyza, D. G. Switching from Reactant to Substrate Engineering in the Selective Synthesis of Graphene Nanoribbons. *J. Phys. Chem. Lett.* **2018**, *9*, 2510–2517.

(34) Bieri, M.; Nguyen, M.-T.; Gröning, O.; Cai, J.; Treier, M.; Aït-Mansour, K.; Ruffieux, P.; Pignedoli, C. A.; Passerone, D.; Kastler, M.; Müllen, K.; Fasel, R. Two-Dimensional Polymer Formation on Surfaces: Insight into the Roles of Precursor Mobility and Reactivity. *J. Am. Chem. Soc.* **2010**, *132*, 16669–16676.

(35) Judd, C. J.; Haddow, S. L.; Champness, N. R.; Saywell, A. Ullmann Coupling Reactions on Ag(111) and Ag(110); Substrate Influence on the Formation of Covalently Coupled Products and Intermediate Metal-Organic Structures. *Sci. Rep.* **2017**, *7*, 14541.

(36) Wang, W.; Shi, X.; Wang, S.; Van Hove, M. A.; Lin, N. Single-Molecule Resolution of an Organometallic Intermediate in a Surface-Supported Ullmann Coupling Reaction. *J. Am. Chem. Soc.* **2011**, *133*, 13264–13267.

(37) Di Giovannantonio, M.; El Garah, M.; Lipton-Duffin, J.; Meunier, V.; Cardenas, L.; Fagot Revurat, Y.; Cossaro, A.; Verdini, A.; Perepichka, D. F.; Rosei, F.; Contini, G. Insight into Organometallic Intermediate and Its Evolution to Covalent Bonding in Surface-Confined Ullmann Polymerization. *ACS Nano* **2013**, *7*, 8190–8198.

(38) Fan, Q.; Wang, C.; Han, Y.; Zhu, J.; Kuttner, J.; Hilt, G.; Gottfried, J. M. Surface-Assisted Formation, Assembly, and Dynamics of Planar Organometallic Macrocycles and Zigzag Shaped Polymer Chains with C-Cu-C Bonds. *ACS Nano* **2014**, *8*, 709–718.

(39) Koch, M.; Gille, M.; Viertel, A.; Hecht, S.; Grill, L. Substrate-Controlled Linking of Molecular Building Blocks: Au(111) vs. Cu(111). *Surf. Sci.* **2014**, *627*, 70–74.

(40) Chen, M.; Shang, J.; Wang, Y.; Wu, K.; Kuttner, J.; Hilt, G.; Hieringer, W.; Gottfried, J. M. On-Surface Synthesis and Characterization of Honeycombene Oligophenylene Macrocycles. *ACS Nano* **2017**, *11*, 134–143.

(41) Fan, Q.; Wang, T.; Dai, J.; Kuttner, J.; Hilt, G.; Gottfried, J. M.; Zhu, J. On-Surface Pseudo-High-Dilution Synthesis of Macrocycles: Principle and Mechanism. *ACS Nano* **2017**, *11*, 5070–5079.

(42) Merino-Díez, N.; Garcia-Lekue, A.; Carbonell-Sanromà, E.; Li, J.; Corso, M.; Colazzo, L.; Sedona, F.; Sánchez-Portal, D.; Pascual, J. I.; de Oteyza, D. G. Width-Dependent Band Gap in Armchair Graphene Nanoribbons Reveals Fermi Level Pinning on Au(111). *ACS Nano* **2017**, *11*, 11661–11668.

(43) Fan, Q.; Liu, L.; Dai, J.; Wang, T.; Ju, H.; Zhao, J.; Kuttner, J.; Hilt, G.; Gottfried, J. M.; Zhu, J. Surface Adatom Mediated Structural Transformation in Bromoarene Monolayers: Precursor Phases in Surface Ullmann Reaction. *ACS Nano* **2018**, *12*, 2267–2274.

(44) Offenbacher, H.; Lüftner, D.; Ules, T.; Reinisch, E. M.; Koller, G.; Puschnig, P.; Ramsey, M. G. Orbital Tomography: Molecular Band Maps, Momentum Maps and the Imaging of Real Space Orbitals of Adsorbed Molecules. *J. Electron Spectrosc. Relat. Phenom.* **2015**, *204*, 92–101.

(45) Koller, G.; Berkebile, S.; Oehzelt, M.; Puschnig, P.; Ambrosch-Draxl, C.; Netzer, F. P.; Ramsey, M. G. Intra- and Intermolecular Band Dispersion in an Organic Crystal. *Science* **2007**, *317*, 351–355.

(46) Mugarza, A.; Mascaraque, A.; Pérez-Dieste, V.; Repain, V.; Rousset, S.; García de Abajo, F. J.; Ortega, J. E. Electron Confinement in Surface States on a Stepped Gold Surface Revealed by Angle-Resolved Photoemission. *Phys. Rev. Lett.* **2001**, *87*, 107601.

(47) Abd El-Fattah, Z. M.; Kher-Elden, M. A.; Piquero-Zulaica, I.; García de Abajo, F. J.; Ortega, J. E. Graphene: Free Electron Scattering Within an Inverted Honeycomb Lattice. *arXiv:1808.06034*

(48) Fan, Q.; Dai, J.; Wang, T.; Kuttner, J.; Hilt, G.; Gottfried, J. M.; Zhu, J. Confined Synthesis of Organometallic Chains and Macrocycles by Cu-O Surface Templating. *ACS Nano* **2016**, *10*, 3747–3754.

(49) Piquero-Zulaica, I.; Lobo-Checa, J.; Sadeghi, A.; Abd El-Fattah, Z. M.; Mitsui, C.; Okamoto, T.; Pawlak, R.; Meier, T.; Arnau, A.; Ortega, J. E.; Takeya, J.; Goedecker, S.; Meyer, E.; Kawai, S. Precise Engineering of Quantum Dot Array Coupling Through Their Barrier Widths. *Nat. Commun.* **2017**, *8*, 787.

(50) Gross, L.; Moll, N.; Mohn, F.; Curioni, A.; Meyer, G.; Hanke, F.; Persson, M. High-Resolution Molecular Orbital Imaging Using a *p*-Wave STM Tip. *Phys. Rev. Lett.* **2011**, *107*, 086101.

(51) Hieulle, J.; Carbonell-Sanromà, E.; Vilas-Varela, M.; Garcia-Lekue, A.; Guitián, E.; Peña, D.; Pascual, J. I. On-Surface Route for Producing Planar Nanographenes with Azulene Moieties. *Nano Lett.* **2018**, *18*, 418–423.

(52) Ohtomo, M.; Sekine, Y.; Hibino, H.; Yamamoto, H. Graphene Nanoribbon Field-Effect Transistors Fabricated by Etchant-Free Transfer from Au(788). *Appl. Phys. Lett.* **2018**, *112*, 021602.

(53) Llinas, J. P. et al. Short-Channel Field-Effect Transistors with 9-Atom and 13-Atom Wide Graphene Nanoribbons. *Nat. Commun.* **2017**, *8*, 633.

(54) Moreno, C.; Vilas-Varela, M.; Kretz, B.; Garcia-Lekue, A.; Costache, M. V.; Paradinas, M.; Panighel, M.; Ceballos, G.; Valenzuela, S. O.; Peña, D.; Mugarza, A. Bottom-Up Synthesis of Multifunctional Nanoporous Graphene. *Science* **2018**, *360*, 199–203.

(55) Fan, Q.; Gottfried, J. M.; Zhu, J. Surface-Catalyzed C-C Covalent Coupling Strategies toward the Synthesis of Low-Dimensional Carbon-Based Nanostructures. *Acc. Chem. Res.* **2015**, *48*, 2484–2494.

(56) Goddard, P.; Schwaha, K.; Lambert, R. Adsorption-Desorption Properties and Surface Structural Chemistry of Bromine on Clean and Sodium-Dosed Ag(111). *Surf. Sci.* **1978**, *71*, 351–363.

(57) Horcas, I.; Fernández, R.; Gómez-Rodríguez, J. M.; Colchero, J.; Gómez-Herrero, J.; Baro, A. M. WSXM: A Software for Scanning Probe Microscopy and a Tool for Nanotechnology. *Rev. Sci. Instrum.* **2007**, *78*, 013705.

(58) Soler, J. M.; Artacho, E.; Gale, J. D.; García, A.; Junquera, J.; Ordejón, P.; Sánchez-Portal, D. The SIESTA Method for *Ab Initio* Order-*N* Materials Simulation. *J. Phys.: Condens. Matter* **2002**, *14*, 2745–2779.

(59) Klimeš, J.; Bowler, D. R.; Michaelides, A. Chemical Accuracy for the Van Der Waals Density Functional. *J. Phys.: Condens. Matter* **2010**, *22*, 022201.

Graphical TOC Entry